Physica C 468 (2008) 985–990

Raman Study of Tb-doped YBCO and Ce-doped GdBCO

S. Mozaffari, M. Akhavan

Magnet Research Laboratory (MRL), Department of Physics, Sharif University of Technology, P.O. Box 11365-9161, Tehran, Iran

ARTICLE INFO

Article history:
Received 26 December 2007
Received in revised form 16 April 2008
Accepted 17 April 2008
Available online 27 April 2008

PACS:
74.72.−h
74.62.Dh
63.20.−e

Keywords:
Raman
High temperature superconductivity

Abstract

The phase formation and the variation of the normal phonon frequencies of high temperature superconductors $YBa_2Cu_3O_{7-\delta}$ and $GdBa_2Cu_3O_{7-\delta}$ upon doping Tb and Ce for Y and Gd, respectively, have been investigated using XRD and Raman spectroscopy measurements. It is found that the increase of doping content causes the formation of impurity phases that can be detected in the XRD and Raman spectra, and results in the suppression of superconductivity. Moreover, analysis of the Raman peaks reveals that substitutions of Tb and Ce for Y and Gd in the parent structure are restricted to low concentrations in favor of impurity island formation.

1. Introduction

Since the discovery of high-T_c superconductivity [1], there has been an explosion of experimental and theoretical studies on these materials. A large number of these studies are restricted to the effects of substitution of rare earth (R) elements for Y that is mostly helpful in understanding the superconducting properties and their dependences on different parameters. Among various isomorphic substitutions possible in $YBa_2Cu_3O_{7-\delta}$, the substitution of Pr [2–4], Ce [5,6], and Tb [7–9], for Y have received the most attention. The reason for this interest is that these substitutions suppress the transition temperature of superconductivity drastically. The $Y_{1-x}Pr_xBa_2Cu_3O_{7-\delta}$ system is particularly interesting since it is isostructural with the $YBa_2Cu_3O_{7-\delta}$ superconductor, yet the superconductivity is strongly suppressed as a function of Pr concentration [4].

Despite the large number of experimental and theoretical reports on doping YBCO with these elements, their destructive effect on superconductivity is still not completely understood. These studies include a number of Raman and infrared spectroscopic investigations that provide an improved understanding of the impurity phases [10], the pair breaking mechanism [11], and the superconducting mechanism itself by either measurement of the superconducting gap [12] or by identification of a strong electron–phonon interaction [13]. Such studies could be very informative because vibrational spectroscopy is an excellent technique for the investigation of low energy elementary excitations in these materials [14]. In order to find a world-class theory for superconductivity, the effects of various parameters, such as doping and oxygen content, on the occurrence or elimination of this phenomenon is examined. There are evidences showing that electron–phonon interaction plays a major role in the occurrence of high-T_c superconductivity [13,15–17]. See also Ref. [18] and the references therein. In this work, we have made an attempt to investigate the effects of Tb and Ce doping on the phonon spectra of the high temperature superconductors YBCO and GdBCO, respectively.

2. Experimental details

Polycrystalline samples of $Y_{1-x}Tb_xBa_2Cu_3O_{7-\delta}$ with Tb content $x = 0$, 0.1, 0.3, 0.5, 0.6, and $Gd_{1-x}Ce_xBa_2Cu_3O_{7-\delta}$ with Ce content $x = 0$, 0.1, 0.3, 0.5, 0.6 were prepared by the solid-state reaction method. For synthesizing the Y series, 99.9% pure Y_2O_3, Tb_4O_7, $BaCO_3$, and CuO powders were mixed in atomic ratios of (Y:Tb):Ba:Cu of 1:2:3. Appropriate amounts of the 99.9% pure Gd_2O_3, CeO_2, $BaCO_3$, and CuO in the stoichiometric ratios were mixed for synthesizing the Gd series. Each mixture was ground and calcinated at 850 °C in air for 24 h. The calcination process was repeated at least twice to ensure sample homogeneity. Then, both of the compounds were pressed into pellets and sintered for 36 h at 950 °C and 930 °C for Y series and Gd series, respectively. Then, the samples were cooled to 450 °C in an oxygen atmosphere, retained there for 5 h, and finally cooled down to room temperature at a cooling rate of 1 °C/min.

* Corresponding author. Tel.: +98 21 66164510; fax: +98 21 66012983.
E-mail address: akhavan@sharif.edu (M. Akhavan).

0921-4534/$ - see front matter © 2008 Published by Elsevier B.V
doi:10.1016/j.physc.2008.04.012

Routine X-ray diffraction measurements were carried out at room temperature using a Philips θ/2θ diffractometer with Cu K_α radiation ($\lambda = 1.5406$ Å) for $Y_{1-x}Tb_xBa_2Cu_3O_{7-\delta}$ polycrystalline samples, and Co radiation ($\lambda = 1.7887$ Å) for $Gd_{1-x}Ce_xBa_2Cu_3O_{7-\delta}$ polycrystalline samples. The cell parameter refinements were performed using the Fullprof software [19].

Raman scattering studies were performed on fresh surfaces. Raman spectra were obtained using a LAB RAM HR800 spectrometer. For Raman excitation the 532 nm line from frequency doubled NdYAG laser was used. The laser was focused to a spot 2 μm in diameter. The Raman scattering measurements were carried out in the spectral region from 200 cm^{-1} and 700 cm^{-1}.

3. Results and discussion

The X-ray diffraction patterns of $Y_{1-x}Tb_xBa_2Cu_3O_{7-\delta}$ samples with $x = 0$, 0.1, 0.3, 0.5, and 0.6 are illustrated in Fig. 1. All samples have the YBCO123 phase which is responsible for the superconducting state. The (200) and (020) peaks near $2\theta \sim 47°$ in the $x = 0$, 0.1, and 0.3 samples are characteristic of the orthorhombic phase. The peak intensities for the YBCO structure are affected by Tb doping, where the intensities of the planes are larger for the pure sample as compared with the doped samples. Upon doping, new secondary phases, like $TbBaO_3$ and $BaCuO_2$, appear in the spectrum. Larger amounts of secondary phases are accompanied by lesser amounts of superconducting phase, which is clearly seen from the growth of the impurity peaks and the depression of the (103) peaks of the superconducting phase.

From the XRD pattern, it is inferred that the solubility of Tb at the Y site is very limited. Single phase compounds result only for $x < 0.3$, whereas the sample with higher Tb content ($x > 0.3$) shows an extra peak at $2\theta \sim 29.5°$ corresponding to the $TbBaO_3$ secondary phase.

The resistivity of the $Y_{1-x}Tb_xBa_2Cu_3O_{7-\delta}$ sample vs. temperature shows that for $x = 0$ the onset transition temperature is $T_C^{onset} \sim 92$ K. The transition temperature remains constant for all samples with $x = 0$–0.5. Mean while, for $x > 0.5$ the superconductivity is suppressed [20]. As the XRD pattern shows, for $x = 0.6$ the amount of YBCO phase is so low that the superconducting grains can not link together, and consequently, superconductivity does not occur.

Further data are captured through the Reitveld analysis. The results of the refinement of the lattice parameters are shown in Fig. 2. With Tb doping, the c parameter of the orthorhombic unit cell is found to decrease continuously with x, in agreement with Ref. [8]; and, while the plane axes of the unit cell i.e., a-, increases slightly with x-, the b-axis does not show any change. In addition, the cell volume V compresses with Tb doping.

Ce substitution for Gd in $Gd_{1-x}Ce_xBa_2Cu_3O_{7-\delta}$ has a considerable effect on the superconducting properties. The superconducting transition temperature gradually decreases with the increasing Ce concentrations [21].

The X-ray diffraction patterns of $Gd_{1-x}Ce_xBa_2Cu_3O_{7-\delta}$ samples with $x = 0$, 0.1, 0.3, and 0.5 are illustrated in Fig. 3. These X-ray patterns are representative of the samples with orthorhombic symmetry, which is responsible for the superconducting state. The (200) and (020) peaks near $2\theta \sim 55°$ for the $x = 0$ and 0.1 samples are characteristic of the existence of the orthorhombic phase. The peak intensity of the GdBCO structure are affected by Ce doping, where the intensity of the superconducting peaks are larger for the pure sample compared with the doped samples. The samples containing higher concentration of Ce ions contain secondary phases besides the $Gd_{1-x}Ce_xBa_2Cu_3O_{7-\delta}$. These phases are identified as $CeBaO_3$ and $BaCuO_2$. As the Ce content increases, these secondary phases also increase.

According to the XRD patterns for $Y_{1-x}Tb_xBa_2Cu_3O_{7-\delta}$ and $Gd_{1-x}Ce_xBa_2Cu_3O_{7-\delta}$, the samples consist of mixed phases containing RBCO (R = Y, Gd), $BaCuO_2$, and $TbBaO_3$/$CeBaO_3$. Clearly, the superconductivity arises from the RBCO phase. For the Pr-doped YBCO system, the XRD results reveal that the samples are orthorhombic with no secondary peaks present [6]. Comparing the XRD spectra of the Pr-doped, Ce-doped, and Tb-doped systems, it can be inferred that for the Ce-doped and Tb-doped systems it is the secondary phase that suppresses the superconducting state, while for the Pr-doped systems other mechanisms should be considered for the suppression of superconductivity.

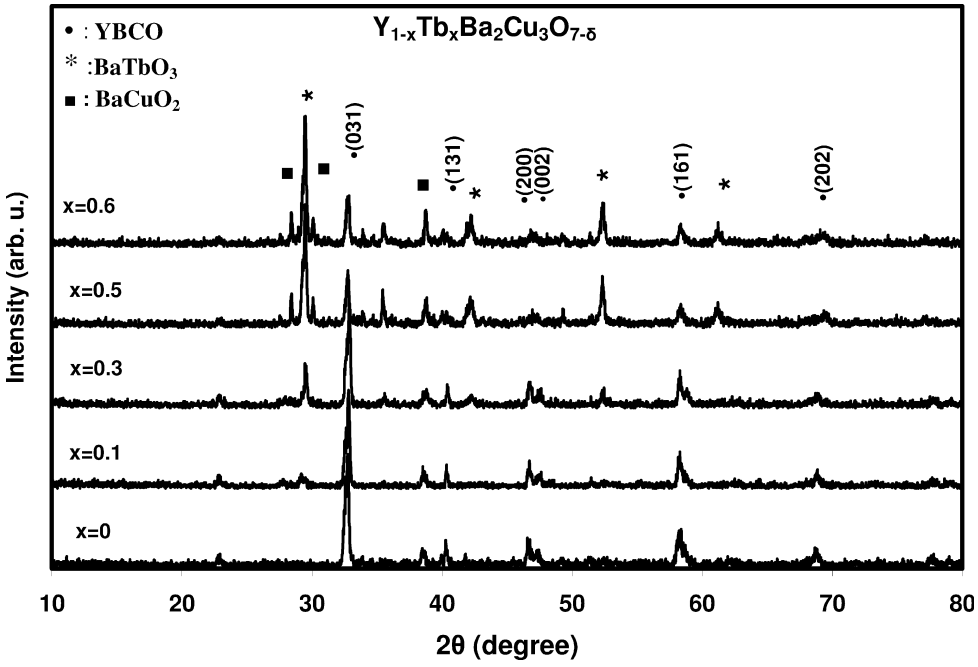

Fig. 1. X-ray diffraction patterns of $Y_{1-x}Tb_xBa_2Cu_3O_{7-\delta}$ for $x = 0$, 0.1, 0.3, 0.5 and 0.6.

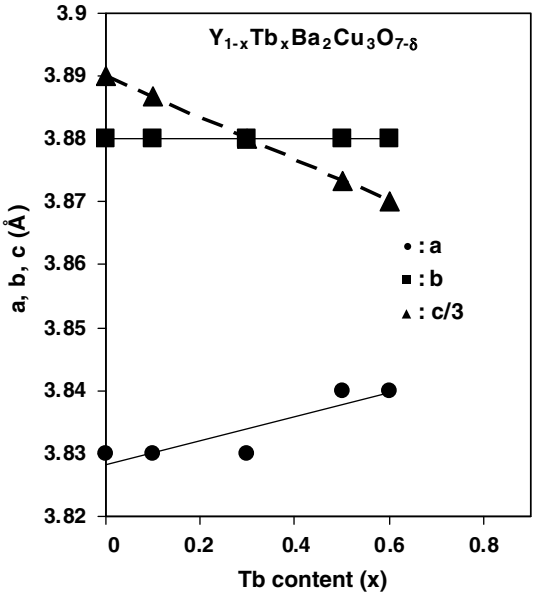

Fig. 2. Lattice parameters a, b and $c/3$ vs. x of $Y_{1-x}Tb_xBa_2Cu_3O_{7-\delta}$.

The lattice parameters a, b, and c, and the cell volume V, obtained from the X-ray diffraction of $Gd_{1-x}Ce_xBa_2Cu_3O_{7-\delta}$ are plotted in Fig. 4 as a function of Ce concentration. The a and b parameters are found to decrease continuously and the c parameter increases with increasing x. While the lattice parameters a and b both decrease, the a parameter decreases rapidly with Ce concentration, and the unit cell volume decreases sharply with the increase of x. The orthorhombic distortion also decreases with increasing Ce substitution. The variation in the c parameter seems reasonable since we have replaced the larger Ce ion for Gd [22]. This increase in the c parameter is consistent with what has been reported for $Y_{1-x}Pr_xBa_2Cu_3O_{7-\delta}$ [23] and $Gd_{1-x}Pr_xBa_2Cu_3O_{7-\delta}$ [24]. The latter reference reports that the replacement of Gd by Pr yields an isotropic expansion of the orthorhombic lattice.

The substitution for lanthanides in the 123 structure unveils the role of impurities on the phonon modes, and provides insights about bond formation. Upon doping the samples with either Tb or Ce, shifts in the frequencies of the normal modes of the superconducting phase, i.e., $YBa_2Cu_3O_{7-\delta}$ or $GdBa_2Cu_3O_{7-\delta}$ are observed. Regarding this, we proceed by studying the modification of the phonon frequencies due to substitution of the rare-earth elements Tb and Ce. The 13 atoms of the orthorhombic unit cell of the superconducting $YBa_2Cu_3O_{7-\delta}$ yield a total of 36 vibrational modes, fifteen modes of which are Raman active. The five A_g Raman-active phonons are as follows: The lowest frequency Raman phonon mode involves mainly the vibrations of the heaviest barium atom, Ba–A_g at 115 cm^{-1}, and the next lowest vibration involves those of the copper atoms, Cu(2)–A_g at 150 cm^{-1}. The remaining three modes are dominated by the vibrations of O(2), O(3), and the apical O(4) oxygen atoms at 340 cm^{-1}, 440 cm^{-1}, and 500 cm^{-1}, respectively. The first two modes involve the out-of-phase vibrations O(2,3)–A_g and the in-phase vibrations O(2,3)–A_g, respectively [25].

Fig. 5 depicts a series of Raman spectra differing in the concentration of Tb. Our edge filter has a detection limit around 200 cm^{-1}, and thus the Ba–A_g mode at 116 cm^{-1} and the Cu(2)–A_g at 150 cm^{-1} are not shown. For the pure sample ($YBa_2Cu_3O_{7-\delta}$), the mode at 500 cm^{-1} is the O(4) stretching mode and the two modes at 339 cm^{-1} and 439 cm^{-1} are the out-of-phase O(2,3)–A_g and the in-phase O(2,3)–A_g modes, respectively. For $x = 0.1$, the spectrum is dominated by the Raman peaks at 337 cm^{-1}, 435 cm^{-1}, and 497 cm^{-1}. For this sample no new Raman peaks are observed in the 200–700 cm^{-1} range, meaning that any new secondary phases make up a very small percentage of the sample.

We note that a shift in the Raman modes is accompanied by Tb substitution for Y. The 30% terbium substituted Raman spectrum shows evidence of Raman modes at 587 cm^{-1} and 632 cm^{-1}. These additional peaks seen in the Raman spectra for $x = 0.3$–0.6, are due to the presence of $BaCuO_2$ phase. $BaCuO_2$ has a strong Raman band about 633 cm^{-1} as well as a broad band about 587 cm^{-1} [26]. Often, the major impurity appears to be $BaCuO_2$ which reflects the

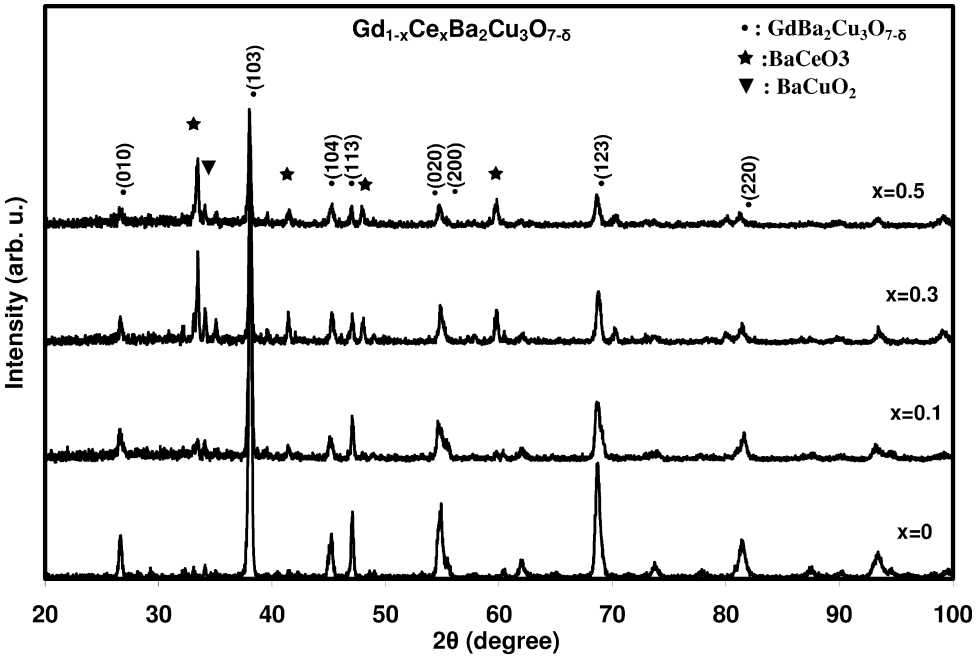

Fig. 3. X-ray diffraction patterns of $Gd_{1-x}Ce_xBa_2Cu_3O_{7-\delta}$ for $x = 0$, 0.1, 0.3 and 0.5.

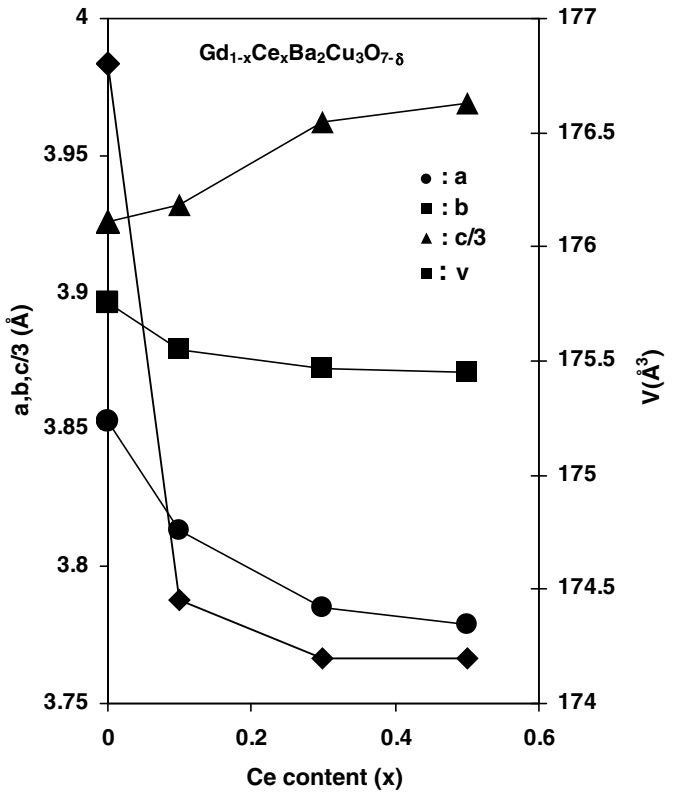

Fig. 4. Lattice parameter a, b and $c/3$ and cell volume V vs. x of $Gd_{1-x}Ce_xBa_2Cu_3O_{7-\delta}$.

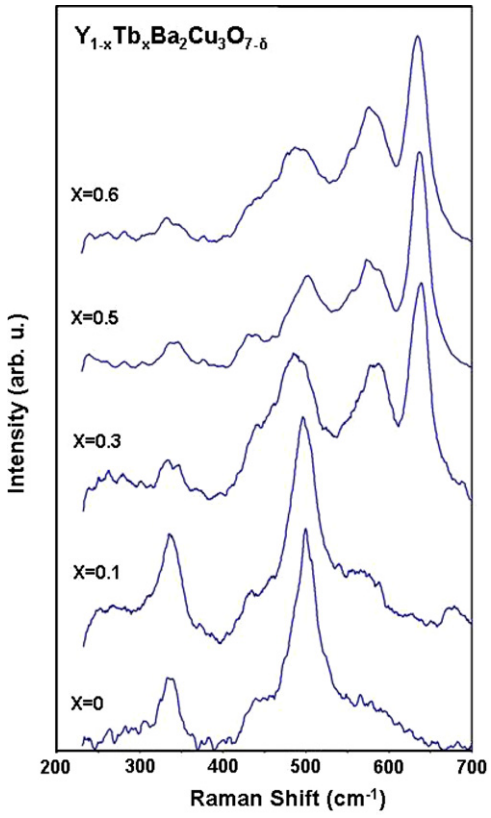

Fig. 5. Raman spectra of $Y_{1-x}Tb_xBa_2Cu_3O_{7-\delta}$ recorded at room temperature.

inherent instability of $YBa_2Cu_3O_{7-\delta}$. Even, small concentrations of this phase can significantly influence the Raman spectra. This insulating material is less absorbing than the superconducting phase and has a large Raman cross section.

There is a small change in the character of the peaks for the $x > 0.3$ sample. The only noticeable change in going to $x > 0.3$ is the considerable reduction in the intensity of the superconducting phase Raman modes. Besides, there is an increase in the peak line width of the superconducting phase, leading to a flat shape. It can be inferred that the peaks contain more than one mode. Our preliminary results indicate a small dependence of the Raman modes of $Y_{1-x}Tb_xBa_2Cu_3O_{7-\delta}$ on higher terbium concentrations. It appears that Tb can replace Y in $YBa_2Cu_3O_{7-\delta}$, to a limited extend, i.e., less than 30%, without producing any impurity phases.

Ref. [27] has investigated the effect of rare earth (R) substitution on the Raman spectra of $RBa_2Cu_3O_{7-\delta}$. The Raman mode for the O(4) stretching vibrations show substantial and systematic variations in vibrational frequency as a function of the ionic rare earth elements. These results are compared to the Cu(1)–O(4) bond-length variation as determined from neutron diffraction studies. It is shown that as the unit cell in the z-direction increases with increasing ionic radii, the Cu(1)–O(4) bond length, which presumably controls the O(4) stretch frequency, increases. We concentrate on the frequency shift of the 500 cm^{-1} mode (see Fig. 6). It seems that the dominant effect on the 500 cm^{-1} mode is caused by the changes in the structural parameters. The observed softening of the O(4) mode is consistent with being the result of the reduction in the c parameter of the unit cell with Tb doping in $YBa_2Cu_3O_{7-\delta}$. It has already been noted that X-ray analysis reveals that the unit cell in the z-direction decreases with increasing terbium concentration.

The substitution of Ce into 123 high temperature superconductors affects significantly the transport properties. Due to this substitution, the metal-superconductor transition takes place at lower temperatures [28]. Broadly speaking, the degradation of transition temperature can be ascribed to the magnetic nature of Ce and its effect on the pair breaking mechanism. It is known that the substitution of Ce^{4+} causes a more stable structure due to Ce4f-O2p hybridization. This hybridization influences the magnetic nature of the ionic Ce, therefore hole filling and pair-breaking are raised [5]. In addition, to get more insight on the effect of this substitution on the vibrational frequencies of the phonon modes due to the difference in the Ce ionic radius, Raman spectroscopy of the structure at different doping content was performed. According to Ref. [29], several phonon lines due to the Raman active A_g symmetry modes were observed at 125 cm^{-1} (barium mode), 153 cm^{-1} (CuO_2-plane copper in-phase mode), 334 cm^{-1} (CuO_2-plane oxygen out-of-phase mode), 449 cm^{-1} (CuO_2-plane oxygen in-phase mode), and 508 cm^{-1} (apical oxygen mode) for the $GdBa_2Cu_3O_{7-\delta}$ orthorhombic structure.

Fig. 7 displays the Raman spectra of $GdBa_2Cu_3O_{7-\delta}$ doped with Ce in the spectral region between 200 cm^{-1} and 700 cm^{-1}. Following Ref. [29], the observed phonons at 326 cm^{-1}, 444 cm^{-1}, and 507 cm^{-1} are the modes of the superconducting phase $GdBa_2Cu_3O_{7-\delta}$. These have been respectively assigned to the out-of-phase O(2,3), in-phase O(2,3), and O(4) stretching modes. The lower wave number modes at 125 cm^{-1} and 151 cm^{-1}, which can be assigned to the A_g vibrations of the Ba and Cu(2), respectively, are not displayed because they are distorted by the notch filter.

The three A_g vibrations described in the preceding paragraph also dominate in $Gd_{0.9}Ce_{0.1}Ba_2Cu_3O_{7-\delta}$, the major differences with respect to GdBCO spectra being a dramatic drop in the intensity of the superconducting phase Raman modes, and the appearance of the secondary phase $BaCuO_2$. The presence of $BaCuO_2$ is revealed through its strong peaks at 587 cm^{-1} and 632 cm^{-1} [26]. In addition, there is a small variation in the Raman modes of the superconducting phase. The O(4) mode shifts to higher frequency on

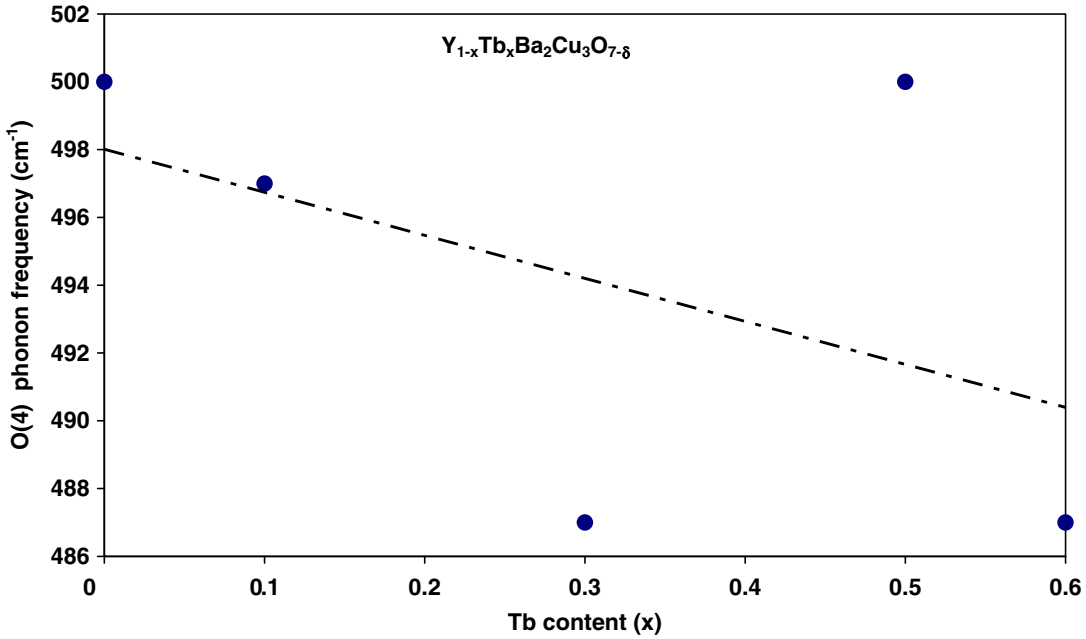

Fig. 6. Apical oxygen O(4) mode frequency of $Y_{1-x}Tb_xBa_2Cu_3O_{7-\delta}$.

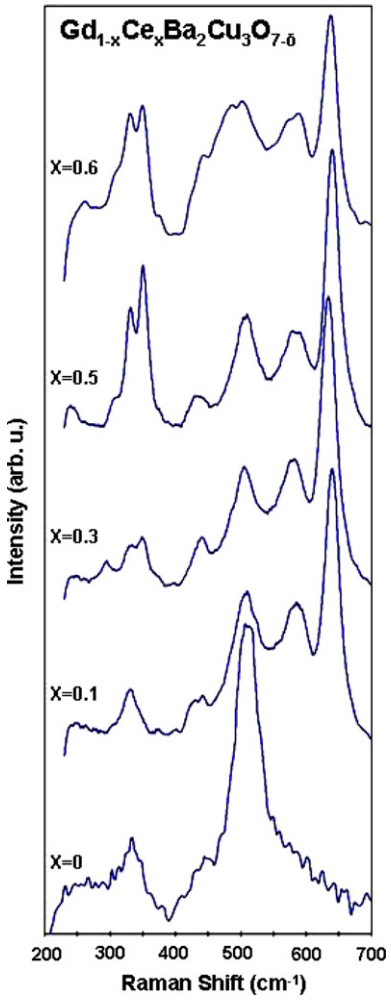

Fig. 7. Raman spectra of $Gd_{1-x}Ce_xBa_2Cu_3O_{7-\delta}$ recorded at room temperature.

going from GdBCO to $Gd_{0.9}Ce_{0.1}Ba_2Cu_3O_{7-\delta}$, and occurs at 511 cm^{-1}. On the other hand, the frequency shifts of the ~330 cm^{-1} and ~444 cm^{-1} modes are small and do not seem to have any obvious systematic variations.

The superconducting Raman modes occur at similar frequencies for $x = 0.3$, 0.5, and 0.6 in $Gd_{1-x}Ce_xBa_2Cu_3O_7$. For $x = 0.3$, there is an overlap between the 330 cm^{-1} intrinsic Raman mode of $Gd_{1-x}Ce_x$-$Ba_2Cu_3O_7$ and the two Raman bands in the region of ~350 cm^{-1}. As the Ce content increases to about 50%, two prominent new Raman bands near ~330 cm^{-1} and 361 cm^{-1} appear in addition to the continuously broadening superconducting phase Raman modes. The Raman bands at 330 cm^{-1} and 361 cm^{-1} are characteristic of the pervoskite nonsuperconducting phase $CeBaO_3$ [30]. All these findings are confirmed by the XRD results, which reveal that Ce could not enter completely into the 123 phase when substituted for Gd to form the Ce123 phase.

In $Gd_{0.9}Ce_{0.1}Ba_2Cu_3O_{7-\delta}$, the substitution of Ce for Gd yields an expansion of the *c*-axis (see Fig. 4). This is expected to result in strengthening of the force constant in the *z*-direction, which would explain the increase of the O(4)–A_g phonon frequency with the increase of Ce concentration. Evolution in the axial phonon frequency i.e., O(4), is in agreement with results of Pr substitution for Y in $Y_{1-x}Pr_xBa_2Cu_3O_{7-\delta}$. The O(4) mode in $Y_{1-x}Pr_xBa_2Cu_3O_{7-\delta}$ is seen to harden some 15 cm^{-1} while the ~340 cm^{-1} mode is seen to soften nearly 40 cm^{-1} in going from $YBa_2Cu_3O_{7-\delta}$ to $PrBa_2$-$Cu_3O_{7-\delta}$. These dominant effects are caused by the larger ionic size of the Pr ion relative to the Y ion [31]. The Ce-doped R123 behaves in a manner similar to the Pr doped R123, that is, as the concentration of the Ce or Pr increases, the normal-state resistivitiy increases and the T_c gradually decreases. This behavior is different in the samples containing Tb; Tb substitution has relatively little or no effect upon T_c. As the Tb concentration increases, the materials remain metallic and T_c remains constant until about $x > 0.5$ where a rapid fall is observed in T_c. Besides, the variations in the main Raman peak of the superconducting phase, O(4), for the Pr doped and Ce doped samples are the same, both increase in frequency. While the similarity of the Ce and Pr is striking, the differences with Tb substitution are obvious, i.e., the O(4) mode decreases in frequency with increasing Tb content. As can be seen in Figs. 5 and 7, none of the superconducting vibrations exhibit any anomalies in their composition dependence that can be associated with the

suppression of superconductivity with the increase of Tb and Ce content in $RBa_2Cu_3O_7$.

4. Conclusions

XRD and Raman analyses were performed to probe the physical properties of the high temperature superconducting $YBa_2Cu_3O_{7-\delta}$ and $GdBa_2Cu_3O_{7-\delta}$ compounds upon addition of Tb and Ce rare earth elements. The XRD analysis shows that in addition to the orthorhombic 123 phase, some nonsuperconducting peaks, which are mainly due to the $BaRO_3$ (R = Tb, Ce) and $BaCuO_2$ secondary phases, are also formed that suppress the superconducting transition temperature. The Rietveld analysis of the XRD patterns reveals a variation in the structural bond formation. In the case of Tb substitution, the *c*-axis of the YBCO unit cell compresses, while in the case of Ce substitution in GdBCO, the *c*-axis compression is drastic.

Raman spectroscopy confirms the XRD phase formations results and shows the dramatic drop in the intensity of the superconducting phase, indicating that part of the 1:2:3 phase has decomposed into $RBaO_3$ (R = Tb,Ce) phases, which compete with the formation of the 1:2:3 structure, thus revealing that the incorporation of Ce and Tb into 1:2:3 is limited to low concentrations. The conductivity in the $Y_{1-x}Tb_xBa_2Cu_3O_{7-\delta}$ pellets is carried along the percolating paths of the Tb poor 1:2:3 phase, embedded in the insolating perv-oskite $TbBaO_3$. At relatively high Tb doping values, the secondary phase formation causes disconnecting of the superconducting grains, and the formation of the superconducting phase (123 phase) is destroyed, consequently the transition temperature for superconductivity disappears.

The Raman data depict that the intrinsic Raman mode near 500 cm^{-1} which is attributed to the O(4) stretching vibration, shows variations in the vibrational frequency as a function of doping. The O(4) stretching mode softens nearly $\sim$13 cm^{-1} on going to 60% increase in the Tb doping content. In the case of Ce doping, the 507 cm^{-1} mode is seen to harden nearly $\sim$4 cm^{-1} on going to 10% increase in the Ce doping content.

Acknowledgments

Fruitful discussions with Dr. M. Noushirvani is acknowledged. We also thank S. Mirshamsi and S. Mofakham for their assistance in sample preparation. This work was supported in part by the Centre of Excellence in Complex Systems and Condensed Matter (CSCM), Department of the Physics, Sharif University of Technology (http://www.cscm.ir).

References

[1] G. Bednorz, K.A. Muller, Z. Phys. B **64** (1986) 18.
[2] M. Akhavan, Physica B **321** (2002) 265.
[3] M. Akhavan, Phys. Status Solidi B **241** (2004) 1242.
[4] D. Palles, D. Lampakis, E. Siranidi, E. Liarokapis, A. Ganatis, M. Calamiotou, Physica C **460** (2007) 922.
[5] C.R. Fincher, Phys. Rev. Lett. **67** (1991) 2902.
[6] L. Shi, Y. Huang, W. Pang, X. Liu, L. Wang, X.G. Li, G. Zhou, Y. Zhang, Physica C **282** (1997) 1021-1022.
[7] S. McCall, G. Cao, F. Freibert, M. Shepard, P. Henning, J.E. Crow, B. Andraka, J. Supercond. **8** (1995) 669.
[8] R.A. Gunasekaran, J.V. Yakhmi, R.M. Iyer, J. Mater. Sci. Lett. **12** (1993) 1151.
[9] U. Staub, M.R. Antonio, L. Soderholm, M. Guillaume, W. Henggeler, A. Furrer, Phys. Rev. B **50** (1994) 7085.
[10] H. Chang, Q.Y. Chen, W.K. Chu, Physica C **309** (1998) 215.
[11] T. Hiramachi, T. Masui, S. Tajima, Physica C **463** (2007) 89.
[12] M.V. Klein, M. Rübhausen, D. Budelmann, B. Schulz, P. Guptasarma, M.S. Williamsen, Ruixing Liang, D.A. Bonn, W.N. Hardy, J. Phys. Chem. Solids 67 (2006) 298.
[13] M.L. Kulic, Phys. Rep. 338 (2000) 1.
[14] M. Cardona, Physica C 317–318 (1999) 30.
[15] G.H. Gweon, T. Sasagawa, S.Y. Zhou, J. Graft, H. Takagai, D.H. Lee, A. Lanzara, Nature 430 (2004) 187.
[16] A. Lanzara, P.V. Bogdanov, X.J. Zhou, S.A. Keller, D.L. Feng, E.D. Lu, T. Yoshida, Z.X. Shen, Nature 412 (2001) 510.
[17] E. Liarokapisa, D. Lampakisa, D. Pallesa, J. Karpinskib, C. Panagopoulos, J. Phys. Chem. Solids 67 (2006) 2065.
[18] H. Khosroabadi, B. Mossalla, M. Akhavan, Phys. Rev. B 76 (2007) 054508.
[19] J. Rodriguez-Carnavajal, Physica B 55 (1993) 192.
[20] S. Mirshamsi, S. Fallahi, S. Mofakham, M. Akhavan, Jpn. J. Appl. Phys., submitted for publication.
[21] S. Mofakham, M. Mazahari, S. Mirashmsi, M. Akhvan, J. Phys.: Condens. Matter, submitted for publication.
[22] R.D. Shannon, Acta Cryst. A 32 (1976) 571.
[23] H.B. Radousky, J. Mater. Res. 7 (1992) 1917.
[24] Z. Yamani, M. Akhavan, Phys. Rev. B 56 (1997) 7894.
[25] S. Hong, K. Kim, H. Cheong, G. Park, Physica C 454 (2007) 82.
[26] H. Chang, Y.T. Ren, Y.Y. Sun, Y.Q. Wang, Y.Y. Xue, C.W. Chu, Physica C 228 (1994) 383.
[27] H.J. Rosen, R.M. Macfarlance, E.M. Engler, V.Y. Lee, R.D. Jacowitz, Phys. Rev. B 38 (1988) 2460.
[28] M. Mazaheri, S. Mofakham, M. Akhavan, Supercond. Sci. Technol., submitted for publication.
[29] T. Kakeshita, K. Horose, S. Lee, Physica C 463 (2007) 96.
[30] H.C. Gupta, P. Simon, T. Pagnier, G. Lucazeau, J. Raman Spectrosc. 32 (2001) 331.
[31] H.B. Radousky, K.F. McCarty, J.L. Peng, R.N. Shelton, Phys. Rev. B 39 (1989) 12383.